



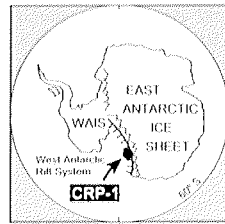
# Petrography, Mineral Chemistry and Provenance of Basement Clasts in the CRP-1 Drillcore (Victoria Land Basin, Antarctica)

F. TALARICO & S. SANDRONI

Dipartimento di Scienze della Terra, Università di Siena, via del Laterino 8, 53100 Siena - Italy

Received 15 July 1998; accepted in revised form 25 October 1998

**Abstract** - Petrographical and mineral chemistry data are described for the most representative basement lithologies occurring as clasts (pebble grain-size class) from the CRP-1 drillcore. Most pebbles consist of either undeformed or foliated biotite with or without hornblende monzogranites. Other rock types include biotite with or without garnet syenogranite, biotite-hornblende granodiorite, tonalite, monzogranitic porphyries, haplogranite, quartz-monzonite (restricted to the Quaternary section), Ca-silicate rocks and biotite amphibolite (restricted to the Miocene strata). The common and ubiquitous occurrence of biotite with or without hornblende monzogranite pebbles, in both the Quaternary and Miocene sections, apparently mirrors the dominance of these rock types in the granitoid assemblages which are presently exposed in the upper Precambrian-lower Palaeozoic basement of south Victoria Land. The other CRP-1 pebble lithologies show petrographical features which consistently support a dominant supply from areas of the Transantarctic Mountains located to the west and south-west of the CRP-1 site, and they thus further corroborate a model of local provenance for the supply of basement clasts to the CRP-1 sedimentary strata.



## INTRODUCTION

This paper presents petrographical and mineral chemistry data on the most representative basement lithologies occurring as clasts (pebble grain-size class) in the Quaternary and lower Miocene sedimentary strata recovered at the first drillsite of the Cape Roberts Project (CRP-1) in the McMurdo Sound, at the southwestern end of the Ross Sea, between the Transantarctic Mountains of south Victoria Land and the recent (<5 Ma) volcanic Ross Island (Cape Roberts Science Team, 1998a, 1998d) (Fig. 1).

This work was initiated with two main tasks, to improve the petrographical characterisation of the basement clasts within the core (Cape Roberts Science Team, 1998b, 1998c) and to better constrain their most likely source rock units within the inland sector of the Transantarctic Mountains facing the CRP-1 area. Because of the relatively small size of most clasts (pebbles with diameters usually below 2-3 cm) and the generally high degree of greenschist facies alteration, geochemical analysis could not be performed. However, microprobe data were obtained on the most representative and least altered samples, including foliated and undeformed biotite monzogranites, a biotite-hornblende granodiorite, a biotite amphibolite and a Ca-silicate rock.

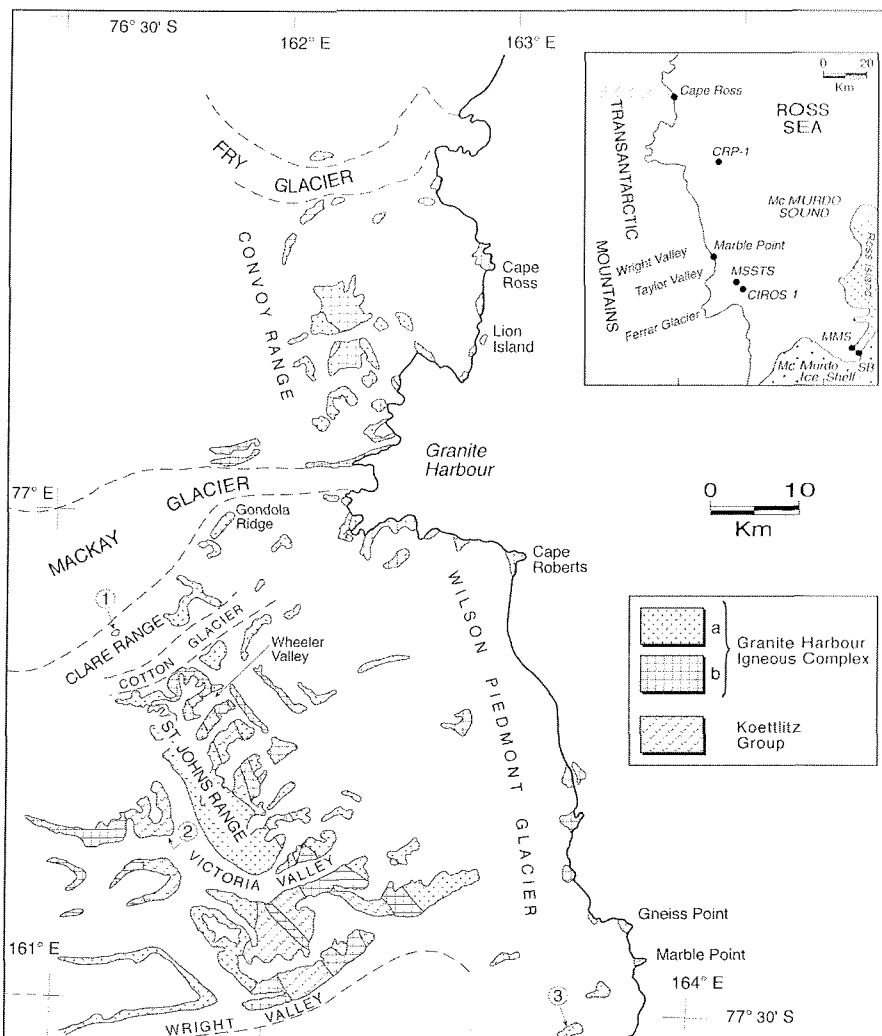
The petrographical comparison between the CRP-1 clast lithologies and those which underlie the present-day sector of the Transantarctic Mountains facing Cape Roberts further corroborates a model of local provenance for the supply of basement clasts in the CRP-1 strata.

## GEOLOGICAL SETTING AND PREVIOUS WORK ON CRP-1 BASEMENT CLASTS

The CRP-1 drillhole is located 16 km ENE of Cape Roberts (Fig. 1) on the western edge of the Victoria Land Basin, the westernmost one of the four main extensional basins making up the Ross Sea continental shelf (Cooper et al., 1994, and references therein). The Victoria Land Basin is bounded on the west by the Transantarctic Mountains which comprise: 1) an upper Precambrian-lower Palaeozoic crystalline basement of granitoid rocks (Granite Harbour Igneous Complex) and metamorphic rocks (Koettlitz Group) (Stump, 1995, and references therein); 2) a quartzose sedimentary cover of Devonian to Triassic age (Beacon Supergroup); and 3) dolerite sills and dykes of Jurassic age (Ferrar Supergroup). Cenozoic alkalic volcanic rocks of the McMurdo Volcanic Group crop out to the east and south of McMurdo Sound.

Results from previous borehole investigations (CIROS-1, MSSTS-1) in McMurdo Sound (Fig. 1) indicated that all these four geological terrains supplied detritus to the Victoria Land Basin. They also provided evidence of significant and persistent influxes of basement-derived pebbles throughout most of the recovered sedimentary strata at the western edge of the basin. The supply of clasts from the upper Precambrian-lower Palaeozoic basement into Quaternary marine sediments in the McMurdo Sound area was previously documented in a short sequence (<10 m) recovered in the MSSTS drillhole, in which granitoid and metamorphic rocks were reported (Barrett et

*Fig. 1* - Generalised geological sketch map of the crystalline basement in the Transantarctic Mountains between Fry Glacier and Wright Valley, to the west of McMurdo Sound (simplified after Gunn & Warren, 1962). Inset shows a schematic map of the southwest corner of the Ross Sea and the location of CRP-1, CIROS-1 and MSSTS-1 drillsites in McMurdo Sound (MMS: McMurdo Station; SB: Scott Base). a = Granite Harbour Igneous Complex: mainly undeformed granitoids; b = Granite Harbour Igneous Complex: predominantly flow-foliated and deformed granitoids. 1, 2, 3 : location of known Ca-silicate rocks with mineral assemblages similar to those of CRP-1 pebbles. 1 = western Clare Range (southern side of Mackay Glacier), 2 = upper Victoria Valley, 3 = Hiorth Hills.



al., 1987). Basement pebbles including granite, granitic gneiss and biotite schist (George, 1989) were recognised as forming a large proportion (35 to 80%) of the clasts in the lower Miocene strata recovered in the CIROS-1 core (Hambrey et al., 1989). Similar contributions were reported in the Miocene record of the MSSTS-1 core (Barrett et al., 1986).

The CRP-1 drillhole recovered a sequence consisting of a Quaternary glacigenic interval down to 43.55 metres below the sea floor (mbsf) and, below this, early Miocene glacigenic sediments down to 147.69 mbsf. A preliminary petrographical characterisation of CRP-1 basement clasts (Cape Roberts Science Team, 1998b, 1998c) was based on macroscopic observations, and led to a preliminary description of all clasts belonging to the granule to cobble grain-size classes (2-256 mm); some inferences concerning the most likely source rock-units were also made.

In the Quaternary part of the CRP-1 core, the content of crystalline basement clasts was found to be range generally from few to 40% of the core by volume. Smaller pebbles and granules were mainly grey biotite granite above 21.90 mbsf, and pink biotite granite in the lower part of the section. Coarser pebbles, mainly confined to diamictites within lithostratigraphic Units 1.1, 2.1, 2.3 and 4.1, were mainly grey biotite granite and, less frequently, other rock types such as fine-grained foliated granitoid

rocks (at 38.04, 42.35 and 43.44 mbsf), biotite haplogranites (20.90 and 30.94 mbsf) and felsic volcanic rocks (at 16.06 mbsf) (Cape Roberts Science Team, 1998b).

In the diamictite units of the CRP-1 lower Miocene interval, basement clasts are present throughout, but show a higher abundance in lithostratigraphic Units 5.3, 5.8, particularly in Units 6.1 and 6.3, where their content ranges up to to 55-60% by volume (*i.e.* at 124.31-126.05 mbsf in Unit 6.3, at 104.55-108.49 mbsf in Unit 6.1). As in the Quaternary strata, finer pebbles and granules were found to consist mainly of grey biotite granite (prevailing in Units 5.2, 5.3, 5.8 -lower part-, 6.1, 6.2. and 6.3) and of pink biotite granite (dominant in Units 5.5 and 5.8 -upper part-, and mixed together with the grey variety in Unit 6.1). For the coarser pebbles, nine rock types were recognised, including dominant grey and pink biotite granites (persistent throughout most of the lithostratigraphic units, with higher abundance in lithostratigraphic Units 6.1 and 6.3), subordinate hornblende-biotite foliated granodiorite and foliated granitoid rocks (restricted to the lower part of the core, below 96.34 mbsf, within Units 5.8 and 6.3), amphibolite (at 138.45 mbsf), Ca-silicate rocks (concentrated in Units 5.2 and 6.3), grey biotite haplogranites (Units 5.3 and 6.3), three porphyritic granitoids (restricted to Units 6.1 and 6.2), and rare pink felsic volcanic rocks.

Tab. 1 - Petrographical classification and mineral assemblages of selected basement clasts from the Quaternary and Miocene sections of the CRP-1 borehole.

Sample code	Top (mbsf)	Clast shape	Approximate size (cm)	Lithology	Mineral assemblage	Lithostratigraphic Unit
TAL61	16.07	rounded	3x2x2	Foliated leucocratic biotite tonalite	Pl (55%), Qtz (40%), Bt (5%), Kfs (t), Chl (s), Ttn (s), Opm (t), Ttn (t), Aln (t), Ap (t), Zrn/Mnz (t)	1.1
TAL62	20.36	subangular	4x3x3	Grey biotite-hornblende quartz-monzonite	Pl (33%), Kfs (30%), green Hbl (14%), Qtz (12%), Bt (11%), Act (s), Ms (s), Chl (s), Ttn (s), Opm (t), Ep (s), Ap (t), Zrn/Mnz (t)	2.1
TAL64	21.90	angular	0.5x1x1	Grey biotite-bearing haplogranite	Kfs (34%), Qtz (33%), Pl (32%), Bt (1%), Ms (s), Chl (s), Ttn (s), Opm (t), Ap (t), Zrn/Mnz (t)	2.1
TAL66	30.62	angular	4x2x2	Grey biotite monzogranite	Pl (34%), Kfs (34%), Qtz (31%), Bt (1%), Opm (t), Ap (t), Chl (s), Ttn (s), Ms (s)	3.1
TAL69	39.45	subrounded	5x6x5	Grey biotite-hornblende monzogranite	Kfs (32%), Pl (31%), Qtz (30%), Bt (4%), green Hbl (2%), Opm (t), Aln (t), Zrn/Mnz (t), Ap (t)	4.1
TAL70	39.74	angular	2x3x2	Clinopyroxene-bearing tonalite	Pl (50%), Cpx (30%), Qtz (20%), green Hbl (s), Opm (s), Chl (s), Zrn/Mnz (t)	4.1
TAL71	40.90	subrounded	5x6x4	Foliated biotite monzogranite	Kfs (33%), Pl (32%), Qtz (31%), Bt (4%), Opm, Ap, Chl (s), Ttn (s), Ms (s)	4.1
TAL14	96.34	angular	1.5x1x1	Biotite-hornblende monzogranite	Pl (35%), Kfs (25%), Qtz (20%), green Hbl (12%), Bt (8%), Opm (t), Zrn/Mnz (t)	5.8
TAL15	103.59	angular	3x4x2	Leucocratic clinopyroxene-biotite granodiorite	Pl (50%), Qtz (30%), Kfs (18%), Cpx (2%), Bt (t), Ms (s), Cal (s), Chl (s), Ttn (t), Opm (t)	5.8/6.1
TAL22	104.76	subrounded	1x3x2	Biotite-hornblende monzogranitic porphyry	Pl (40%), Kfs (28%), Qtz (25%), Bt (4%), green Hbl (2%, s), Cpx (1%), Ms (s), Opm (t), Zrn (t), Ap (t)	6.1
TAL23	104.99	angular	6x4x3	Grey biotite monzogranite	Qtz (34%), Pl (33%), Kfs (31%), Bt (2%), Ms (s), Chl (s), Opm (t), Aln (t), Zrn (t)	6.1
TAL24	105.88	angular	4x3x3	Pink biotite-hornblende monzogranite	Kfs (39%), Qtz (34%), Pl (25%), Bt (1%), Hbl (1%), Ms (s), Ep (s), Chl (s), Aln (t), Opm (t)	6.1
TAL27	108.10	angular	3x2x2	Grey biotite monzogranite	Kfs (35%), Qtz (33%), Pl (31%), Bt (1%), Ms (s), Chl (s), Opm (t), Zrn/Mnz (t)	6.1
TAL29	108.49	angular	3x2x3	Biotite-bearing monzogranitic porphyry	Qtz (37%), Pl (31%), Kfs (29%), Bt (2%), Opm (1%), Ms (s), Cal (s), Chl (s), Opm (t), Ttn (t), Zrn (t)	6.1
TAL30	115.06	angular	5x6x4	Grey biotite monzogranite	Qtz (34%), Pl (32%), Kfs (32%), Bt (2%), Ms (s), Chl (s), Opm (t), Zrn (t)	6.2
TAL31	117.04	angular	3x6x4	Biotite-hornblende tonalite	Pl (47%), Qtz (22%), Bt (15%), green Hbl (9%), Cpx (6%), Kfs (1%), Ms (s), Chl (s), Ttn (t), Opm (t), Ap (t), Aln (t), Zrn/Mnz (t)	6.2
TAL35	121.84	subrounded	2x1x2	Pink biotite monzogranite	Kfs (34%), Qtz (33%), Pl (32%), Bt (1%), Ms (s), Chl (s), Ttn (s), Opm (t), Aln (t)	6.3
TAL41	124.76	rounded	6x3x4	Yellowish-grey biotite haplogranite	Qtz (34%), Pl (32%), Kfs (32%), Bt (2%), Ms (s), Chl (s), Opm (t), Zrn/Mnz (t)	6.3
TAL44	125.40	rounded	5x0.5x3	Garnet-bearing biotite syenogranite	Kfs (43%), Qtz (40%), Pl (17%), Bt (t), Grt (t), Opm (t), Ms (s), Zrn/Mnz (t)	6.3
TAL45	125.87	angular	2x1x1	Pink monzogranitic porphyry	Pl (40%), Qtz (35%), Kfs (25%), Bt (t), Ms (s), Chl (s), Ttn (s), Cal (s)	6.3
TAL46	128.59	subrounded	3x1x1	Pink biotite-hornblende monzogranite	Kfs (38%), Qtz (34%), Pl (25%), Bt (2%), green Act-Hbl (1%), Ms (s), Cbl (s), Aln (t), Opm (t), Ap (t), Zrn/Mnz (t)	6.3
TAL49	131.98	subrounded	3x2x4	Pink foliated biotite monzogranite	Qtz (42%), Kfs (30%), Pl (27%), Bt (1%), Opm (t), Ms (s), Chl (s), Ttn (s), Zrn/Mnz (t)	6.3
TAL50	132.71	subrounded	3x1x1.5	Grey foliated biotite monzogranite	Pl (34%), Kfs (32%), Qtz (31%), Bt (3%), Ms (s), Chl (s), Prh (s), Ttn (s), Opm (t), Aln (t), Ap (t), Zrn/Mnz (t)	6.3
TAL51	134.51	subrounded	4x3x1.5	Pink biotite-hornblende monzogranite	Kfs (38%), Qtz (31%), Pl (28%), Bt (2%), Hbl (1%), Ms (s), Chl (s), Opm (t), Zrn/Mnz (t)	6.3
TAL52	134.71	subangular	4x3x2	Biotite-hornblende granodiorite	Pl (45%), Qtz (30%), Kfs (10%), green Hbl (9%), Bt (6%), Ms (s), Aln (t), Ap (t), Zrn/Mnz (t)	6.3
TAL53	134.96	subangular	5x3x3	Grey biotite monzogranite	Kfs (35%), Qtz (33%), Pl (30%), Bt (2%), Ms (s), Chl (s), Opm (t), Aln (t), Ap (t), Zrn/Mnz (t)	6.3
TAL54	135.33	subrounded	3x4x3	Ca-silicate rock and margin of a granitic vein	Ca-silicate rock: Pl (30%), Qtz (30%), Cpx (25%), Bt (15%), Act-Hbl (s), Ms (s), Chl (s), Ttn (t), Opm (t), Zrn/Mnz (t); Grt-bearing monzogranitic vein: Qtz (40%), Pl (25%), Kfs (24%), Grt (1%), Ms (s), Chl (s), Opm (t)	6.3
TAL56	137.62	angular	3x2x1	Grey biotite monzogranite	Pl (38%), Qtz (34%), Kfs (25%), Bt (3%), Ms (s), Chl (s), Ttn (s), Opm (t), Ap (t), Zrn/Mnz (t)	6.3
TAL57	138.45	angular	3x2x1	Biotite-bearing amphibolite	Pl (45%), green Hbl (40%), Bt (10%), Qtz (5%), Ms (s), Chl (s), Prh (s), Ap (t), Ttn (t), Opm (t)	6.3

Note: mineral abbreviations are according to Kretz (1983). Mineral phases are listed in order of decreasing abundance, and the modal contents of essential phases are given as percentages, t = trace (<1% modal content), s = mineral phase of secondary origin. Lithostratigraphic unit designation follows Cape Roberts Science Team (1998a; Fig. 18).

## PETROGRAPHICAL FEATURES AND MINERAL CHEMISTRY

### PETROGRAPHY

Representative samples are listed in table 1 to illustrate the lithological range and mineral assemblages typical of basement clasts from the Quaternary and lower Miocene sections of the CRP-1 borehole. The petrographical analysis of CRP-1 basement clasts revealed the occurrence of a variably developed, but commonly extensive, alteration. It is particularly advanced in the dominant clasts of igneous rocks but also evident in the few clasts of metamorphic rocks. The mineral transformations which affected the primary mineral assemblages show microstructural features typical of static, strain-free transformations (pseudomorphs and reaction rims). They include the partial to complete replacement of calcic plagioclase by saussurite (sericite-albite±epidote±calcite), K-feldspar by sericite or kaolinite micro-aggregates, red-brown biotite by Fe-Mg or Mg-Fe chlorite and/or prehnite + titanite ± opaque minerals, and Mg-hornblende by actinolite and/or chlorite. All these mineral phases are diagnostic of low-temperature, greenschist to sub-greenschist facies conditions. It is noteworthy that the colour distinction between grey and pink granites mainly reflects differences in the degree of low temperature alteration, which is commonly more advanced in pink (or red-coloured) granitoid rocks than in the grey varieties. The relation between the degree of reddening of the K-feldspars and advanced hydrothermal alteration resulting in sericitization and introduction of Fe-Ti oxides, was documented by Craw & Frindlay (1984), who also suggested a causal relationship with the regional, Jurassic thermal event associated with the intrusion of the Ferrar Dolerite.

Most pebbles previously classified as grey and pink biotite granites (Cape Roberts Science Team, 1998b, 1998c) are monzogranites, including both undeformed biotite- (30.62, 104.99, 108.10, 115.06, 121.84, 124.76, 134.51 mbsf) and biotite-hornblende- (39.45, 96.34, 105.88, 126.05, 134.51 mbsf) bearing varieties, as well as foliated biotite types (40.90, 131.98, 132.71, 137.62 mbsf) with or without hornblende.

In all the undeformed monzogranites, grain-sizes range from fine- to medium/coarse, and textures are equigranular to heterograngular and hypidiomorphic. Mineral assemblages (Tab. 1) include alkali feldspar (microperthitic orthoclase or microcline, often as poikilitic phenocrysts and transformed into a felty micro-aggregate of kaolinite or sericite), plagioclase (oligoclase-andesine displaying a marked normal compositional zoning and partly transformed into sericite or saussurite), quartz, red-brown or dark olive green biotite (in places replaced by Fe-Mg-chlorite±prehnite±epidote) (Fig. 2a), with or without green hornblende (Fig. 2b), opaque minerals (commonly ilmenite), apatite, monazite/zircon and allanite.

The foliated monzogranites show fabrics characterised either by parallel alignment of unstrained grains of twinned plagioclase and biotite (indicative of magmatic flow), or by the preferential dimensional orientation of biotite

lamellae, which wrap around strained feldspar grains (Fig. 2c), and by internal ductile deformation within mineral grains such as subgrain boundaries, wavy extinction, kink-bands and deformation twins. These features are all indicative of solid-state deformation.

Other rock types are much less common and include: biotite syenogranites (4 pebbles), garnet-bearing biotite syenogranites (1), biotite-hornblende granodiorite (1), leucocratic clinopyroxene-bearing granodiorite (1), foliated leucocratic tonalite (1), clinopyroxene-bearing tonalite (1), clinopyroxene-hornblende-biotite tonalite (1), monzogranitic porphyries (3) and haplogranites (1), quartz-monzonite (1), Ca-silicate rocks (3) and biotite amphibolites (1).

Biotite syenogranites (55.54, 79.11, 108.19, and 125.14 mbsf) are equigranular to heterograngular, medium to coarse grained, and hypidiomorphic. Their mineral assemblages are similar to those of biotite monzogranites except for the higher modal content of alkali-feldspar (microcline) and the rare occurrence of small euhedral garnet crystals in one sample (125.40 mbsf).

Biotite-hornblende granodiorite (134.71 mbsf) is heterograngular, fine to medium-grained and hypidiomorphic; subhedral to euhedral laths of plagioclase are normally zoned (an39-35) or have patchy zoning structures, and contain fine-grained inclusions of biotite and hornblende; quartz occurs as interlobate granular aggregates, and K-feldspar (perthitic orthoclase) forms either poikilitic phenocrysts or interstitial grains. Both biotite and hornblende show a weak dimensional preferred orientation. The leucocratic clinopyroxene-bearing variety (103.59) is strongly altered and medium to coarse grained with allotriomorphic texture: clinopyroxene crystals mainly occur within finer-grained domains composed of plagioclase (an36), quartz and minor biotite and titanite.

Foliated leucocratic tonalite (16.07 mbsf) shows a marked foliation defined by parallel alignment of plagioclase (an32) laths, red-brown biotite lamellae and quartz polycrystalline aggregates: both biotite and plagioclase show prominent kink-bands and quartz typically occurs as highly strained grains mantled by sub-polygonal aggregates of finer-grained new grains; a late generation of green biotite forms very fine grained lamellae which grew along fractures and cataclastic bands. Clinopyroxene-bearing varieties (39.74, 117.04 mbsf) are undeformed and characterised by medium grain sizes with equigranular, hypidiomorphic to micrographic textures, the latter defined by plagioclase (an42)-quartz intergrowth. In these rocks, clinopyroxene forms anhedral crystals, partly to completely replaced by green hornblende with or without chlorite, and typical accessory phases include titanite and allanite.

Grey biotite-bearing haplogranites (*e.g.* 21.90 mbsf) are very fine- to fine-grained, with interlobate to sub-polygonal granular textures, low modal contents of red-brown biotite, and poikilitic grains of microcline containing rounded inclusions of quartz, oligoclase and green-brown biotite partly replaced by Fe-Mg chlorite ± prehnite.

Biotite±hornblende±clinopyroxene-bearing monzogranitic porphyries (108.49, 104.76, 125.87 mbsf) are characterised by euhedral phenocrysts of orthoclase/

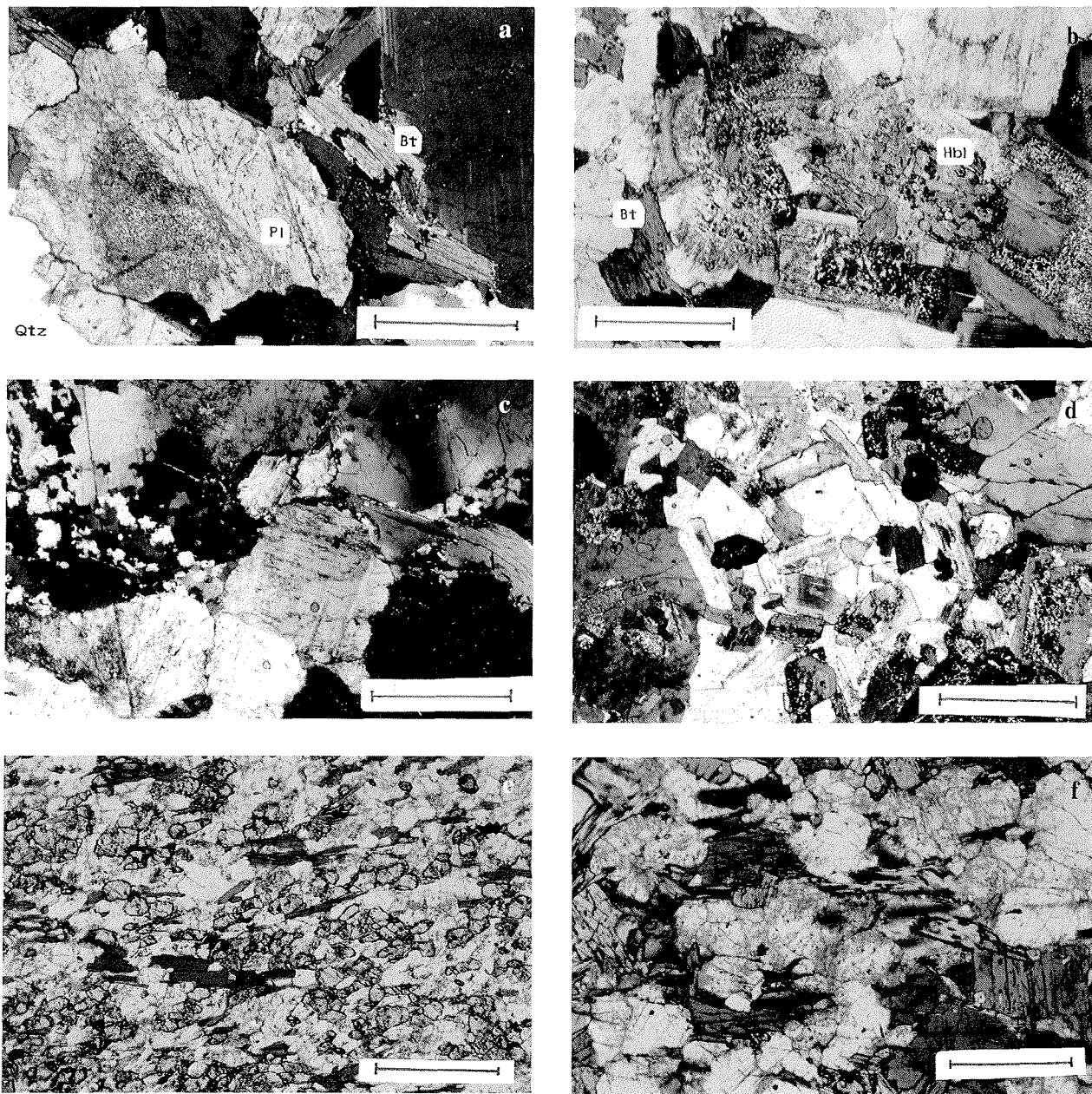


Fig. 2 - Photomicrographs of the principal basement rock types in the CRP-1 core. *a)* Grey biotite monzogranite (TAL23, 104.99 mbsf), hypidiomorphic/allotriomorphic texture with sericitised plagioclase (Pl), chloritised biotite flakes (Bt) and interstitial quartz (Qtz). Crossed nicols, scale bar = 2 mm. *b)* Pale pink biotite-hornblende monzogranite (TAL24, 105.88 mbsf); hypidiomorphic texture with euhedral laths of saussuritised plagioclase, chloritised hornblende (Hbl) and biotite flakes (Bt). Crossed nicols, scale bar = 2 mm. *c)* Foliated biotite monzogranite (TAL71, 40.90 mbsf). The foliation is defined by biotite flakes and warps around partly recrystallised plagioclase grains. Crossed nicols, scale bar = 2 mm. *d)* Grey biotite-hornblende quartzo-monzonite (TAL62, 20.36 mbsf). Crossed nicols, scale bar = 2 mm. *e)* Ca-silicate rock (TAL54, 135.33 mbsf): this rock consists of a fine-grained granoblastic aggregate of diopside and plagioclase, plus biotite. Plane-polarised light, scale bar = 2 mm. *f)* Biotite-bearing amphibolite (TAL57, 138.45 mbsf). Nematoblasts of green hornblende and flakes of chloritised biotite define a weak foliation. Plane-polarised light, scale bar = 2 mm.

microcline (microperthitic and replaced by clay mineral micro-aggregates or sericite), sericitised oligoclase, quartz, clinopyroxene (augite) and brown to green hornblende, often forming glomeroporphyritic aggregates and set within a fine to very-fine grained felsic groundmass consisting of plagioclase, quartz and K-feldspar with scattered aggregates of red-brown biotite, opaque minerals, titanite and white mica. In Sample 108.49 mbsf, feldspar pheno-crystals are fragmented and contain microfractures filled by the felsic groundmass, suggesting that the rock suffered brittle

deformation before the groundmass had fully crystallised.

Quartz-monzonite (20.36 mbsf) is very altered, heterograniular, fine to medium grained and hypidiomorphic-poitikilitic; plagioclase occurs as sub-idiomorphic grains showing oscillatory zoning and andesine (an38) cores associated with patchy zoning structures; both perthitic K-feldspar and quartz are present as poikilitic crystals carrying inclusions of plagioclase, biotite (transformed to chorite ± epidote) and green hornblende (replaced by actinolite ± chlorite) (Fig. 2d).

The three samples of Ca-silicate rocks (61.52, 126.76, 135.33 mbsf) are fine grained with a marked foliation defined by clinopyroxene and biotite. The foliation is parallel to a millimetre-scale compositional layering composed of alternating layers of granoblastic plagioclase, quartz and clinopyroxene, and plagioclase, quartz, clinopyroxene and biotite (or K-feldspar) ± green hornblende/actinolite (Fig. 2e). Clinopyroxene (salite) is locally transformed into actinolite pseudomorphs. Accessory minerals include abundant titanite (2%) and rare ilmenite. A garnet-bearing monzogranitic vein was observed in Sample 135.33 mbsf: the vein cross cut the metamorphic fabric at high angle and it has a fine to medium grained, allotriomorphic texture. Garnet (unzoned alm54-sps37-grs8-pyrl) occurs as euhedral crystals which are partly replaced by chlorite ± epidote.

The biotite amphibolite (138.45 mbsf) is fine/medium-grained and shows a granonematoblastic texture defined by the preferential dimensional orientation of green hornblende and biotite (partly replaced by chlorite, titanite and prehnite) (Fig. 2f).

#### MINERAL CHEMISTRY

Five of the least altered samples were selected for mineral analysis. They comprise two Quaternary samples (foliated monzogranite 40.90 mbsf, TAL71, and undeformed monzogranite 30.62 mbsf, TAL66) and three from the lower Miocene section (biotite-hornblende granodiorite 134.71 mbsf, TAL52; Ca-silicate rock 135.33 mbsf, TAL54, and biotite amphibolite 138.45 mbsf, TAL57) (Tab. 1). Chemical analyses of the main mineral phases were carried out with an X-ray energy dispersive system EDAX DX4 attached to a Scansion Electron Microscope Philips XL30, at 20 Kv, 60 µA of emission

current and a beam spot size of 0.2 µm, using natural minerals as standards.  $\text{Fe}_2\text{O}_3$  in clinoamphiboles and clinopyroxenes was calculated assuming charge balance and using the equation given by Papike et al. (1974).

**Biotite** - Representative analyses of biotite are listed in table 2. No significant intra-crystalline compositional variations were detected. In the two monzogranites (TAL66 and TAL71), the biotite composition is characterised by  $\text{Al}^{\text{IV}}$  from 2.45 to 2.55 (atoms per formula unit, a.p.f.u., on the base of 22 oxygens) and  $X_{\text{Fe}}$  variable from 0.68 to 0.62. Biotite grains occurring as inclusion within K-feldspar phenocrysts commonly show the highest  $X_{\text{Fe}}$  (Tab. 2). The granodiorite (TAL52) is characterised by biotite with lower  $X_{\text{Fe}}$  (Fig. 3). In both the foliated monzogranite (TAL71) and the granodiorite recrystallized grains usually show lower  $X_{\text{Fe}}$  and higher  $\text{Al}^{\text{IV}}$  contents with respect to primary crystals (Tab. 2). In the  $\text{FeO}-\text{MgO}-\text{Al}_2\text{O}_3$  diagram (Rossi & Chevremont, 1987) (Fig. 4) sample data predominantly plot in the calc-alkaline field. A few data from sample TAL66 fall in the alumino-potassic field, possibly reflecting more advanced chloritisation of the analysed crystals. Biotite from the two metamorphic rocks show very limited compositional variations:  $X_{\text{Fe}} = 0.51-0.52$ ,  $\text{Al}^{\text{IV}} 2.45-2.50$  in biotite amphibolite (TAL57) and  $X_{\text{Fe}} = 0.44-0.45$ ,  $\text{Al}^{\text{IV}} 2.28-2.29$  in the Ca-silicate rock (TAL54).

**Clinoamphibole and Clinopyroxene** - Representative analyses are listed in table 3. In the samples, the amphiboles are members of the calcic-amphibole group (Leake, 1978) and they are mainly Mg-hornblende, with the exception of the Ca-silicate rock (TAL54) in which the late amphibole replacing clinopyroxene is actinolite with  $X_{\text{Mg}}$  around 0.62 (Fig. 5). In granodiorite (TAL52) and biotite-amphibolite (TAL57), slight zoning was detected with  $X_{\text{Mg}}$  ranging from 0.55 to 0.57 and from 0.54 to 0.60, respectively, from core to rim (Tab. 3). Clinopyroxene

Tab. 2 - Representative chemical analyses of biotite in CRP-1 basement clasts TAL66 (grey biotite monzogranite), TAL71 (foliated biotite monzogranite), TAL52 (biotite-hornblende granodiorite), TAL57 (biotite-bearing amphibolite) and TAL54 (Ca-silicate rock).

Oxide (wt%)	TAL66				TAL71				TAL52		TAL57		TAL54		
	1	2	3-i	4-i	1	2-i	3-n	4-n	1	2-n	1	2	1	2	
$\text{SiO}_2$	35.88	35.68	35.93	36.35	35.53	35.69	35.76	35.76	36.24	36.34	38.54	37.01	36.46	38.42	38.24
$\text{Al}_2\text{O}_3$	17.48	17.59	17.01	17.12	17.20	17.29	16.99	17.43	14.70	15.68	16.02	15.64	15.37	15.27	
$\text{TiO}_2$	3.41	3.57	3.55	3.38	3.07	3.20	2.72	1.65	4.12	5.19	3.77	3.92	1.83	1.62	
$\text{MgO}$	6.35	6.69	6.42	6.75	6.81	6.34	7.49	8.36	9.54	9.41	10.43	10.68	12.86	13.03	
$\text{FeO}$	23.36	23.02	23.90	23.03	23.75	24.11	24.57	23.97	21.48	18.31	20.42	19.99	18.33	18.84	
$\text{MnO}$	0.46	0.46	0.51	0.50	0.41	0.56	0.44	0.46	0.21	0.11	0.20	0.27	0.16	0.27	
$\text{K}_2\text{O}$	9.38	9.22	9.28	9.35	9.15	9.26	8.71	8.01	9.27	8.80	9.29	9.40	9.50	9.33	
$\text{Na}_2\text{O}$	0.26	0.62	0.23	0.27	0.54	0.43	0.22	0.56	0.07	0.39	0.00	0.34	0.32	0.13	
$\text{CaO}$	0.00	0.10	0.00	0.00	0.10	0.07	0.00	0.14	0.00	0.26	0.00	0.12	0.09	0.00	
Total	96.58	96.95	96.84	96.75	96.57	96.95	96.89	96.81	95.73	96.70	97.13	96.81	96.87	96.73	
Structural formulae on the basis of 22 oxygens															
Si	5.504	5.450	5.512	5.552	5.469	5.481	5.482	5.518	5.582	5.977	5.549	5.502	5.716	5.707	
$\text{Al}^{\text{IV}}$	2.496	2.550	2.488	2.448	2.531	2.519	2.518	2.482	2.418	2.023	2.451	2.498	2.284	2.293	
$\text{Al}^{\text{VI}}$	0.665	0.617	0.588	0.635	0.590	0.611	0.553	0.647	0.244	0.844	0.381	0.284	0.412	0.394	
Ti	0.393	0.410	0.410	0.388	0.355	0.370	0.314	0.189	0.476	0.605	0.425	0.445	0.205	0.182	
Mg	1.452	1.523	1.468	1.537	1.562	1.451	1.711	1.897	2.184	2.175	2.330	2.402	2.851	2.898	
Fe	2.997	2.941	3.066	2.942	3.058	3.097	3.150	3.052	2.760	2.375	2.560	2.523	2.281	2.352	
Mn	0.060	0.060	0.066	0.065	0.053	0.073	0.057	0.059	0.027	0.014	0.025	0.035	0.020	0.034	
K	1.836	1.797	1.816	1.822	1.797	1.814	1.703	1.556	1.817	1.741	1.777	1.810	1.803	1.777	
Na	0.077	0.184	0.068	0.080	0.161	0.128	0.065	0.165	0.021	0.117	0.000	0.099	0.092	0.038	
Ca	0.000	0.016	0.000	0.000	0.016	0.012	0.000	0.023	0.000	0.043	0.000	0.019	0.014	0.000	
Total	15.479	15.546	15.482	15.469	15.593	15.555	15.554	15.589	15.529	15.914	15.499	15.616	15.679	15.675	
$X_{\text{Fe}}$	0.67	0.66	0.68	0.66	0.66	0.68	0.65	0.62	0.56	0.52	0.52	0.51	0.44	0.45	

Note: i = inclusion in K-feldspar; n = recrystallised grains marking a sub-solidus foliation. Total Fe as  $\text{FeO}$ .  $X_{\text{Fe}} = \text{Fe}^{2+}/(\text{Fe}^{2+} + \text{Mg})$ .

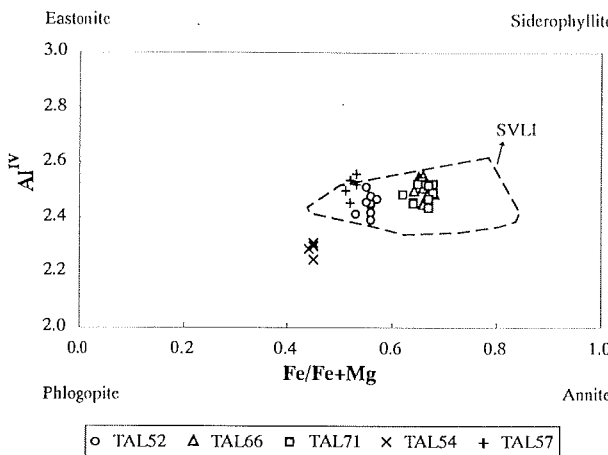


Fig. 3 - Biotite composition in terms of  $\text{Al}^{\text{IV}}$  vs  $\text{Fe}/(\text{Fe}+\text{Mg})$  for CRP-1 basement clasts TAL66 (grey biotite monzogranite, 30.62 mbsf), TAL71 (foliated biotite monzogranite, 40.90 mbsf), TAL52 (biotite-hornblende granodiorite, 134.71 mbsf), TAL57 (biotite-bearing amphibolite, 138.45 mbsf) and TAL54 (Ca-silicate rock, 135.33 mbsf). Outlined field is that of biotite compositions from the calc-alkaline South Victoria Land Intrusives (Armienti et al., 1990) on the basis of data reported in Biagini et al. (1991).

(TAL54) is salite and shows intra-crystalline compositional variations from wo<sub>49</sub>-en<sub>32</sub>-fs<sub>19</sub> (core) to wo<sub>48</sub>-en<sub>28</sub>-fs<sub>24</sub> (rim).

**Feldspars** - Representative compositions of plagioclase are listed in table 4. In biotite monzogranite (TAL66), plagioclase shows normal zoning and ranges in composition from an<sub>39</sub> (core) to an<sub>23</sub> (rim). In foliated biotite monzogranite (TAL71), the composition is more sodic, from an<sub>25</sub> (core) to an<sub>23</sub> (rim) for the phenocrysts, and from an<sub>24</sub> to an<sub>16</sub> for the recrystallised grains which define the subsolidus foliation. Plagioclase from granodiorite (TAL52) ranges in composition from an<sub>39</sub>

(core) to an<sub>35</sub> (rim). No significant zoning was detected in plagioclase grains from the biotite amphibolite (TAL57) (an<sub>41</sub>-40), whereas plagioclase from the Ca-silicate rock (TAL54) has a wider compositional variation in the range from an<sub>59</sub>-60 (core) to an<sub>38</sub>-27 (rim). Microperthitic K-feldspar from plutonic samples is characterised by bulk microperthite compositions in the range or<sub>88</sub>-ab<sub>12</sub> to or<sub>90</sub>-ab<sub>10</sub> (TAL66 and TAL52), and or<sub>85</sub>-ab<sub>14</sub>-an<sub>1</sub> to or<sub>82</sub>-ab<sub>17</sub>an<sub>1</sub> (TAL71), with a compositional range of the potassic phase from or<sub>88</sub> to or<sub>98</sub>.

## COMPARISON WITH ON-SHORE BASEMENT ROCK TYPES AND CONCLUSIONS

Preliminary investigations on CRP-1 basement clasts (Cape Roberts Project Team, 1998b, 1998c) indicated that several basement lithologies were involved as sources of clasts in the CRP-1 drillhole. A major source was identified in rock-units belonging to the Cambro-Ordovician Granite Harbour Igneous Complex (Gunn & Warren, 1962; Allibone et al., 1993a, 1993b), which forms the most extensive outcrop of crystalline basement in southern Victoria Land (Fig. 1).

In particular, three main sources were inferred on the basis of the dominant lithologies in the core and comparison with on-shore geological data: i) post-tectonic granitoid rocks, including either discordant plutons (for grey biotite monzogranites) or dyke swarms (for haplogranites and porphyritic granitoids) (e.g. "post-tectonic granitoid rocks", such as the "Irizar Granite" of Gunn & Warren, 1962); ii) concordant elongated plutons consisting of flow-foliated or deformed granitoid rocks ("pre-tectonic gneiss" and "syn-tectonic granitoid rocks", e.g. "Larsen Granodiorite", of Gunn & Warren, 1962); and, restricted to the pebbles of the Miocene section, iii) metamorphic rocks of the amphibolite facies Koettlitz Group (for Ca-silicate rocks and biotite amphibolite) (Grindley & Warren, 1964; Williams et al., 1971; Findlay et al., 1984; Allibone, 1992).

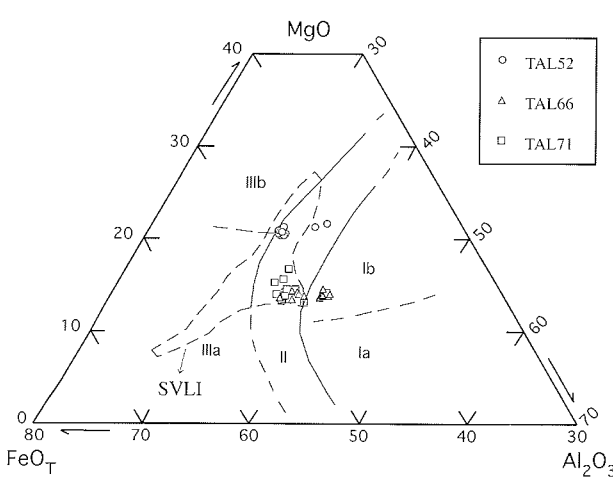


Fig. 4 - Ternary  $\text{FeO}_\text{T}$ - $\text{MgO}$ - $\text{Al}_2\text{O}_3$  diagram for biotites (after Rossi & Chevremont, 1987) from CRP-1 plutonic clasts TAL66 (grey biotite monzogranite, 30.62 mbsf), TAL71 (foliated biotite monzogranite, 40.90 mbsf) and TAL52 (biotite-hornblende granodiorite, 134.71 mbsf). Field I: "Aluminopotassique" association (Ia: type Limousine; Ib: type Guèret); field II: Calc-alkaline association; field III: Monzonitic association (IIIa: Fe-potassic; IIIb: Mg-potassic). The field of biotite compositions from the calc-alkaline South Victoria Land Intrusives is also indicated (data of Biagini et al., 1991).

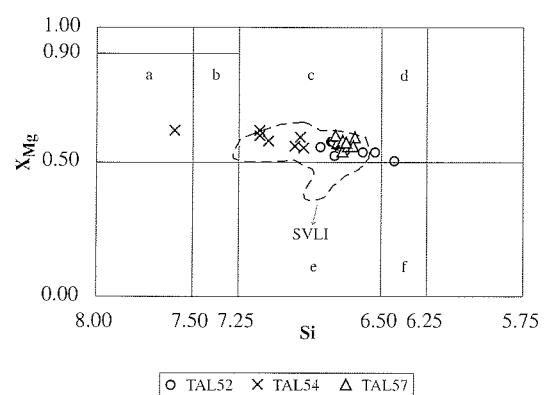


Fig. 5 - Ca-amphiboles classification (after Leake, 1978) for CRP-1 samples TAL52 (biotite-hornblende granodiorite, 134.71 mbsf), TAL57 (biotite-bearing amphibolite, 138.45 mbsf) and TAL54 (Ca-silicate rock, 135.33 mbsf). ( $\text{Ca} + \text{Na})/\text{B} > 1.34$ ,  $(\text{Na} + \text{K}) < 0.50$ . a: actinolite; b: actinolitic hornblende; c: Mg-hornblende; d: tschermackitic hornblende; e: Fe-hornblende; f: Fe-tschermarkitic hornblende. The field of amphibole compositions from the calc-alkaline South Victoria Land Intrusives is also shown (data of Biagini et al., 1991).

Tab. 3 - Representative chemical analyses of hornblende and clinopyroxene in CRP-1 basement clasts TAL52(biotite-hornblende granodiorite), TAL57 (biotite-bearing amphibolite) and TAL54 (Ca-silicate rock).

Oxide (wt%)	TAL52		Clinoamphibole		TAL54		Clinopyroxene	
	1-c	2-r	1-c	2-r	1	2	1-c	2-r
SiO <sub>2</sub>	45.07	45.54	45.07	45.71	51.96	46.52	52.63	52.10
Al <sub>2</sub> O <sub>3</sub>	9.16	8.47	10.95	9.92	3.87	8.89	1.03	1.00
TiO <sub>2</sub>	1.40	1.28	1.31	1.27	0.10	0.31	0.10	0.00
Fe <sub>2</sub> O <sub>3</sub>	5.18	6.06	0.76	3.67	0.68	2.05	0.00	0.00
MgO	9.63	10.04	9.99	10.74	13.06	10.49	10.80	9.20
FeO	14.16	13.53	15.34	12.86	14.36	15.21	11.88	14.48
MnO	0.51	0.34	0.20	0.38	0.54	0.49	0.21	0.23
CaO	11.01	11.00	11.32	11.25	11.96	11.68	23.00	22.56
Na <sub>2</sub> O	1.53	1.36	1.72	1.43	0.86	1.31	0.35	0.42
K <sub>2</sub> O	0.83	0.80	1.01	0.80	0.43	1.23	0.00	0.00
Total	98.48	98.42	94.94	95.80	96.53	95.64	100.00	100.00
Structural formulae on the basis of 23 oxygens (amphibole) and 6 oxygens (pyroxene)								
Si	6.699	6.757	6.703	6.737	7.587	6.908	1.993	1.997
Al <sup>IV</sup>	1.301	1.243	1.297	1.263	0.413	1.092	0.007	0.003
Al <sup>VI</sup>	0.304	0.239	0.622	0.461	0.253	0.464	0.039	0.042
Ti	0.157	0.143	0.147	0.141	0.011	0.035	0.003	0.000
Fe <sup>3+</sup>	0.580	0.676	0.085	0.407	0.074	0.229	0.000	0.000
Mg	2.134	2.220	2.214	2.359	2.841	2.321	0.610	0.525
Fe <sup>2+</sup>	1.760	1.679	1.908	1.585	1.754	1.889	0.376	0.464
Mn	0.064	0.042	0.025	0.048	0.067	0.062	0.007	0.007
Ca	1.754	1.749	1.804	1.777	1.871	1.859	0.933	0.926
Na	0.441	0.391	0.496	0.408	0.244	0.377	0.026	0.031
K	0.157	0.152	0.192	0.151	0.080	0.233	0.000	0.000
Total	15.351	15.291	15.493	15.337	15.195	15.469	3.994	3.996
X <sub>Mg</sub>	0.55	0.57	0.54	0.60	0.62	0.55	-	-
en%	-	-	-	-	-	-	32	28
fs%	-	-	-	-	-	-	19	24
wo%	-	-	-	-	-	-	49	48

Note: c = core composition; r = rim composition.

The new petrographical and mineral chemistry data provide further support for these conclusions. The abundance throughout the drillcore of pebbles of undeformed, biotite and biotite-hornblende monzogranites mirrors the dominance of these rock types in the upper Precambrian-lower Palaeozoic basement of South Victoria Land (Allibone et al., 1991; Allibone et al., 1993a; Pocknall et al., 1994; Isaac et al., 1995), particularly the Dry Valleys 2 (DV2) and Dry Valleys 1b (DV1b) suites, respectively, of Smillie (1992) and Allibone et al. (1993b). Biotite monzogranites crop out extensively at Gondola Ridge and in the St. John's Range (they are major constituents of the DV1b; e.g. Suess and St. John's plutons; Allibone et al., 1993b), and hornblende-biotite monzogranites are the dominant lithology in the eastern St. John's Range in the Wheeler Valley (the DV2 - discordant Swinford Pluton of Allibone et al., 1993a) and in Granite Harbour (e.g. Lion Island; Graham & Palmer, 1987).

The microstructural characteristics of the foliated granitoid pebbles closely resemble those of granitoids

forming the early DV1a concordant plutons (such as the Wheeler Pluton in the Mackay Glacier region or the Bonney Pluton in the Dry Valleys-Blue Glacier region, Allibone et al., 1993b) which show well-developed magmatic flow fabrics and, at some margins, overprinted solid-state fabrics (Cox, 1993).

The biotite syenogranite pebbles could have been sourced in either DV2 or DV1b plutons (see Fig. 8 in Allibone et al., 1993b), but the lack of hornblende suggests a more likely derivation from the DV1b suite. Biotite-hornblende granodiorites have been reported as a major rock type within DV1a plutons of the Dry Valleys - Ferrar region (e.g. Bonney Pluton). Although they are generally flow-foliated (Cox, 1993; Allibone et al., 1993a), a poor foliation is also present in the CRP-1 pebbles.

Flow-foliated tonalites were reported by Smillie (1987) in the cliffs west of the Rhone Glacier (Taylor Valley), whereas the quartz-monzonite pebble in CRP-1 may have been derived from quartz-monzonite sills (or possibly the Pearse Pluton) which are exposed in the area between

Tab. 4 - Representative plagioclase compositions in CRP-1 basement clasts TAL66 (grey biotite monzogranite), TAL71 (foliated biotite monzogranite), TAL52 (biotite-hornblende granodiorite), TAL57 (biotite-bearing amphibolite) and TAL54 (Ca-silicate rock).

	TAL66		TAL71			TAL52		TAL57		TAL54					
	1-c	2-r	1-c	2-r	3-i	4-n	5-n	1-c	2-r	1-c	2-r	1-c/Cpx	2-r/Cpx	3-c/Cam	4-r/Cam
ab%	60	76	73	76	74	83	75	59	63	57	58	40	60	39	71
an%	39	23	25	23	23	16	24	39	35	41	40	59	38	60	27
or%	1	1	2	1	3	1	1	2	2	2	2	1	2	1	2

Note: c = core composition; r = rim composition; i = inclusion in K-feldspar; n = recrystallised grains marking a sub-solidus foliation; /Cpx, /Cam = grain in contact with clinopyroxene, clinoamphibole.

Taylor and Wright Valley (Allibone et al., 1991; Allibone et al., 1993a).

The pebbles of monzogranitic to monzonitic porphyries could reflect minor contributions from Vanda felsic porphyry dykes (Allibone et al., 1991), which form intense dike swarms throughout the Mackay Glacier–Ferrar Glacier region and in the Convoy Range (Pocknall et al., 1994). The haplogranite pebbles resemble the leucocratic biotite granite dykes which predate the emplacement of the Vanda felsic porphyry dykes (Allibone et al., 1993a) and they are widespread in the region.

According to Allibone et al. (1993a), DV1a and possibly DV1b granitoid rocks may represent a southern extension of the South Victoria Land Intrusives (as defined by Armienti et al., 1990). Mineral chemistry data on this meta-alluminous suite are available for the northermost segment (between Cape Irizar and the Priestley Glacier, northern Victoria Land) (Biagini et al., 1991). Most of the biotite compositions of monzogranite pebbles (TAL71 and TAL66) and of granodiorite pebble (TAL52) plot in the compositional field of biotites from the South Victoria Land Intrusives (Figs. 3 & 4). Hornblende compositions in the granodiorite pebble are also closely comparable to those of granodiorites in the South Victoria Land Intrusives (Fig. 5).

Both Ca-silicate rocks and biotite amphibolites are common lithologies within the metasedimentary Koettlitz Group (Williams et al., 1971; Findlay et al., 1984). The assemblage clinopyroxene (wo 0.48–0.49 –fs 0.24–0.21–en 0.26–0.27) + clinoamphibole (Mg-Hbl) + plagioclase + biotite + quartz is typical of Ca-silicate rocks from the region between Ferrar and Koettlitz Glaciers (Williams et al., 1971; authors' unpublished data), as well as forming smaller outcrops in the western Clare Range (southern side of Mackay Glacier), in the upper Victoria Valley and at Hiorth Hills (Fig. 1). Available P-T estimates for Koettlitz Group metasediments indicate peak metamorphic conditions of  $700 \pm 50^\circ\text{C}$  and  $4.5 \pm 1$  kbar, within the upper amphibolite facies (Allibone, 1992). The pebbles of metamorphic rocks within the CRP-1 core have mineral assemblages which are consistent with upper amphibolite facies metamorphic conditions but are generally unsuitable for precise P-T determination. However, application of the Blundy & Holland (1990) plagioclase-amphibole thermometer to the biotite amphibolite (TAL57) yielded temperature values of  $756$ – $745^\circ\text{C}$  (core-rim, respectively) which are consistent with values derived for the Koettlitz Group.

In conclusion, detailed petrographical and mineral analytical comparison between CRP-1 clasts and lithologies which are widely exposed in the Transantarctic Mountains facing the Cape Roberts drillsite strongly support the previous suggestions of a local provenance for basement clasts in the CRP-1 sequence.

#### ACKNOWLEDGEMENTS

We are very grateful to D.N.B. Skinner and J.L. Smellie for reviews and improvements of the manuscript. This work has been carried out as part of the Italian *Programma Nazionale di Ricerche in Antartide*. The Cape Roberts Project was made possible by the resources and close collaboration of the Antarctic

programmes of Italy, New Zealand, United States of America, Germany, Australia and Great Britain, with field operations organised by Antarctica New Zealand. We wish to thank those involved in the field phase of the project for their efforts in recovering the core and related data, and the International Steering Committee for access to the core material.

#### REFERENCES

- Allibone A.H., 1992. Low pressure/high temperature metamorphism of Koettlitz Group schists in the Taylor Valley and Ferrar Glacier regions. *New Zealand Journal of Geology & Geophysics*, **35**, 115–127.
- Allibone A.H., Forsyth P.J., Sewell R.J., Turnbull I.M. & Bradshaw M.A., 1991. Geology of the Thundergut area, southern Victoria Land, Antarctica, 1: 50000. *New Zealand Geological Survey Miscellaneous Geological Map 21* (map and notes), Wellington, New Zealand, Department of Scientific and Industrial Research.
- Allibone A.H., Cox S.C., Graham I.J., Smillie R.W., Johnstone R.D., Ellery S.G. & Palmer K., 1993a. Granitoids of the Dry Valleys area, southern Victoria Land, Antarctica: field relationships, and isotopic dating. *New Zealand Journal of Geology & Geophysics*, **36**, 281–291.
- Allibone A.H., Cox S.C. & Smillie R.W., 1993b. Granitoids of the Dry Valleys area, southern Victoria Land: geochemistry and evolution along the early Paleozoic Antarctic Craton margin. *New Zealand Journal of Geology & Geophysics*, **36**, 299–316.
- Armienti P., Ghezzo C., Innocenti F., Manetti P., Rocchi S. & Tonarini S., 1990. Isotope geochemistry and petrology of granitoid suites from Granite Harbour Intrusives of the Wilson Terrane, north Victoria Land, Antarctica. *European Journal of Mineralogy*, **2**, 103–123.
- Barrett P.J., McKelvey B.C. & Walker B.C., 1986. Sand provenance. *New Zealand DSIR Bulletin*, **237**, 137–144.
- Barrett P.J., Elston D.P., Harwood D.M., McKelvey B.C. & Webb P.N., 1987. Mid-Cenozoic record of glaciation and sea level change on the margin of the Victoria Land basin, Antarctica. *Geology*, **15**, 634–637.
- Biagini R., Di Vincenzo G. & Ghezzo C., 1991. Mineral chemistry of metalluminous granitoids between the David and Campbell Glaciers, Victoria Land (Antarctica). *Memorie della Società Geologica Italiana*, **46**, 231–247.
- Blundy J. D. & Holland T. J. B., 1990. Calcic amphibole equilibria and a new amphibole-plagioclase geothermometer. *Contribution to Mineralogy and Petrology*, **104**, 208–224.
- Cape Roberts Science Team, 1998a. Background to CRP-1, Cape Roberts Project, Antarctica. *Terra Antartica*, **5**(1), 1–30.
- Cape Roberts Science Team, 1998b. Quaternary strata in CRP-1, Cape Roberts Project, Antarctica. *Terra Antartica*, **5**(1), 31–62.
- Cape Roberts Science Team, 1998c. Miocene strata in CRP-1, Cape Roberts Project, Antarctica. *Terra Antartica*, **5**(1), 63–124.
- Cape Roberts Science Team, 1998d. Summary results from CRP-1, Cape Roberts Project, Antarctica. *Terra Antartica*, **5**(1), 125–138.
- Cooper A.K., Brancolini G., Behrendt J.C., Davey F.J., Barrett P.J. & ANTOSTRAT Ross Sea regional working group, 1994. A Record of Cenozoic Tectonism throughout the Ross Sea and Possible Controls on the Glacial Records. In: Cooper A.K., Barker P.F., Webb P.N. & Brancolini G. (eds.), *The Antarctic Continental Margin: Geophysical and Geological Stratigraphic Records of Cenozoic Glaciation, Paleoenvironments, and Sea-Level Change*, *Terra Antartica Spec. Vol.*, **1**(2), 353–355.
- Cox S.C., 1993. Inter-related plutonism and deformation in South Victoria Land, Antarctica. *Geological Magazine*, **130**, 1–14.
- Craw D. & Findlay R.H., 1984. Hydrothermal alteration of Lower Ordovician granitoids and Devonian Beacon Sandstone at Taylor Valley, McMurdo Sound, Antarctica. *New Zealand Journal of Geology & Geophysics*, **27**, 537–550.
- Findlay R.H., Skinner D.N.B. & Craw D., 1984. Lithostratigraphy and structure of the Koettlitz Group, McMurdo Sound, Antarctica. *New Zealand Journal of Geology & Geophysics*, **27**, 513–536.

- George A., 1989. Sand provenance. *New Zealand DSIR Bulletin*, **245**, 159-167.
- Graham I.J. & Palmer K., 1987. New precise Rb-Sr mineral and whole-rock dates of I-type granitoids from Granite Harbour, South Victoria Land, Antarctica. *New Zealand Antarctic Record*, **8(1)**, 72-80.
- Grindley G.W. & Warren G., 1964. Stratigraphic nomenclature and correlation in the western part of the Ross Sea. In: Adie R.J. (ed.), *Antarctic Geology*, North Holland Publishing Co., Amsterdam, 314-333.
- Gunn B.M. & Warren G., 1962. Geology of Victoria Land between the Mawson and Mulock Glaciers, Antarctica. *New Zealand Geological Survey Bulletin*, **71**.
- Hambrey M.J., Barrett P.J. & Robinson P.H., 1989. Stratigraphy. In: Barrett P.J. (ed.), *Antarctic Cenozoic history from the CIROS-1 drillhole, McMurdo Sound, New Zealand*. *DSIR Bulletin*, **245**, 23-48.
- Isaac M.J., Chinn T.J., Edbrooke S.W. & Forsyth P.J., 1995. Geology of the Olympus Range area, southern Victoria Land, Antarctica. Scale 1: 50000. *Institute for Geological & Nuclear Sciences geological map 20*, 1 sheet and 60 p. Institute for Geological & Nuclear Sciences Ltd, Lower Hutt, New Zealand.
- Kretz R., 1983. Symbols for rock forming minerals. *American Mineralogist*, **68**, 277-279.
- Leake B., 1978. Nomenclature of amphiboles. *Mineralogica and Petrographica Acta*, **22**, 195-224.
- Papike J.J., Cameron K.L. & Baldwin K., 1974. Amphiboles and clinopyroxenes. Characterization of other than quadrilateral components and estimates of ferric iron from microprobe data. *Geological Society of America Abstracts Programs*, **6**, 1053-1054.
- Pocknall D.T., Chinn T.J., Sykes R. & Skinner D.N.B., 1994. Geology of the Convoy Range area, southern Victoria Land, Antarctica. Scale 1: 50000. *Institute for Geological & Nuclear Sciences Geological Map 11.1 Sheet and 36 p.* Institute for Geological & Nuclear Sciences Ltd, Lower Hutt, New Zealand.
- Rossi P. & Chevremont P., 1987. Classification des associations magmatiques granitoides. *Geochronique*, **21**, 14-18.
- Smillie R.W., 1987. Petrological evolution of basement granitoids, southern Victoria Land. *New Zealand Antarctic Record*, **8(1)**, 61-71.
- Smillie R.W., 1992. Suite subdivision and petrological evolution of granitoids from the Taylor Valley and Ferrar Glacier region, south Victoria Land. *Antarctic Science*, **4**, 71-87.
- Stump E., 1995. *The Ross Orogen of the Transantarctic Mountains*. Cambridge University Press, Cambridge, 249 p.
- Williams P.E., Hobbs B.E., Vernon R.H. & Anderson D.E., 1971. The structural and metamorphic geology of basement rocks in the McMurdo Sound area, Antarctica. *Journal of the Geological Society of Australia*, **18**, 127-142.